TRAgen: A Tool for Generation of Synthetic Time-Lapse Image Sequences of Living Cells

Vladimír Ulman(✉), Zoltán Orémuš, and David Svoboda

Centre for Biomedical Image Analysis, Masaryk University,
Botanická 68a, 602 00 Brno, Czech Republic
{ulman,xoremus,svoboda}@fi.muni.cz
http://cbia.fi.muni.cz

Abstract. In biomedical image processing, correct tracking of individual cells is important task for the study of dynamic cellular processes. It is, however, often difficult to decide whether obtained tracking results are correct or not. This is mainly due to complexity of the data that can show hundreds of cells, due to improper data sampling either in time or in space, or when the time-lapse sequence consists of blurred noisy images. This prohibits manual extraction of reliable ground truth (GT) data as well. Nonetheless, if reliable testing data with GT were available, one could compare the results of the examined tracking algorithm with the GT and assess its performance quantitatively.

In this paper, we introduce a novel versatile tool capable of generating 2D image sequences showing simulated living cell populations with GT for evaluation of biomedical tracking. The simulated events include namely cell motion, cell division, and cell clustering up to tissue-level density. The method is primarily designed to operate at inter-cellular scope.

Keywords: Biomedical imaging · Simulation · Evaluation · Cell tracking

1 Introduction

The present biomedical research increasingly relies on automated processing and analysis of large amount of image data, which are nowadays commonly produced by the vast majority of acquisition devices. Two fundamental tasks in this area are image segmentation and motion tracking. The task of segmentation is to split the image into several disjoint regions. Depending on the application, the regions can be whole cells, various intra-cellular objects (e.g., mitochondria or some proteins), cell nuclei themselves, or intra-nuclei objects (e.g., chromatin territories or individual genes). The task of motion tracking is to provide links between these regions between consecutive images in the acquired time-lapse sequence. This allows for description of events and changes in the characteristics of studied objects over a period of time. Of course, such analyses should be performed over significantly large datasets, thus in an unsupervised manner. This, however, calls for proper validation, in terms of precision and accuracy, of

V. Murino and E. Puppo (Eds.): ICIAP 2015, Part I, LNCS 9279, pp. 623–634, 2015.
DOI: 10.1007/978-3-319-23231-7_56

the image analysis methods prior to their use in practice. In particular, we will focus on quality examination of cell and cell nuclei tracking algorithms.

For proper evaluation one needs to possess reliable and complete ground truth data (GT), which is a sequence of labelled mask images and corresponding cell lineage trees in the case of cell and nuclei tracking. When seeking for GT for one's particular application, one may ask a human expert to annotate her existing images in order to turn them into a GT dataset. But this is often very tedious and unreliable [27], especially in the 3D case. It is also possible to use some of the existing publicly available datasets. Unfortunately, none of the popular ones [3,8,13,21] offers time-lapse data, except, to the best of our knowledge, for the recent one [16]. Another, and recently becoming particularly popular, solution is to make use of a simulator, which we understand as a tool for generating pseudo-real synthetic testing images accompanied with the GT data, e.g., labelled mask images.

1.1 Current Approaches to Analysis of Tracking Performance

Dufour et al. [4] can be considered to belong among the first research groups that were creating synthetic time-lapse sequences of moving cells for evaluation of tracking performance. In their work, only two spheres were positioned randomly under constraint that they can't overlap and that they touch at least once during the sequence. The images of the spheres were then covered with noise. Later on, the same authors [5] elaborated further their idea in order to yield yet more realistic image sequences.

Other significant contributions [7,11,14] to the field as well as many other researchers relied on expert manual annotation of small subsets of available data. This is somewhat surprising provided that simulated data are often used for evaluating segmentation algorithms. One conclusion we may draw from it is that tracking developers lack reasonable aid for creating one's own synthetic time-lapse images.

Looking into the field of image registration, some authors [12,26] reported recently to obtain synthetic images with elaborate non-rigid object shape changes and realistic texture. Here, the image sequences were created by iteratively preparing image transformations, that introduced various types of motion and deformations, and by applying them on a given initial real image. These methods require, therefore, a sample real image and transformations either measured from real data [26] or synthetic ones [12]. One of the first attempts to put synthetic cells to motion according to fully synthetic transformations, was drafted in [24]. The authors initially filled a mask with a procedural texture [17] to mimic a chromatin structure. The structure was then iteratively transformed with generated smooth vector fields in the course of time. Such approaches can, however, display only limited number of cells, usually only a single one, in the image sequence, which is usually short as well.

In this paper, we would like to fill the gap in the evaluation of tracking algorithms and offer researchers a tool that creates for them image data with populations of realistically living, thus moving and splitting, cells with GT.

1.2 Background on Biomedical Image Simulation

As presented in [23], every simulator can be clearly split into three principal phases: (I) digital phantom object generation, (II) simulation of signal transmission through an optical system, and (III) simulation of signal detection and image formation in an image sensor. In this paper, we introduce a tool capable of generating the appropriate phantom data accompanied with the relevant GT. In this sense, the topic covers the first phase. The remaining two phases are beyond the scope of this text. For further reading, see [15,23]. We would like to emphasize, that we use the term digital phantom instead of model. This comes from our need to avoid association with a comprehensive and the most correct description of an object of interest (that a model would be), quite often devised to have a predictive potential to discover new biology-relevant findings. Our idea is to focus only on the object properties that may influence our observation (the visual experience) in optical microscopy. In fact, the observation is subject to the last two phases. The second phase (II) typically comprises of convolution with a point spread function, often modelled with Gaussian blur, while the third phase (III) typically adds several types of noise to the image. See Ref. [23] for detailed explanation and Ref. [24] for an extension of the three-phase model for time-lapse datasets.

Unlike the majority of simulation toolboxes whose structure can be decomposed into the three consecutive phases, the learning-based approaches employ generative modelling methods or machine learning approaches. These techniques have been recently surveyed in [2].

The credibility of synthetically generated datasets comes from how closely the simulation procedures in all three phases mimic the real data and the simulated system. When creating the digital phantom of cells and cell populations, we need to deal with the following three aspects:

- mutual positions of individual cells,
- cell shape,
- and cell internal texture.

In the rest of the paper, we would like to focus on the former two aspects. These can be represented with cell masks in the synthetic time-lapse image sequence, and they can provide the complete tracking GT. The initial shape of cells, of course, depends on the simulated cell line. We were experimenting with shapes based on the idea that the z-projection of human somatic cells is topologically equivalent to a circle. Hence, the basic initial shape was generated as a slightly deformed ellipse. The fundamental ideas how to prepare a computer generated large cell population were presented by Lehmussola et al. [10]. They were placing individual cells repeatedly until suitable position and allowed overlap were established. The ideas defined in their paper influenced many other authors [15,18,22,28].

Regarding the time-lapse development of cell mask positions within the images, we propose a concept adopted from the field of crowd motion simulations (see the recent review [6]). In particular, it is extending the popular

social force model [9] mainly in the three aspects. First, cells, which correspond to pedestrians in terms of their model, can split or naturally die during the simulation. Second, cells can take different shape and change its shape during simulation, in contrast to modelling all pedestrians with fixed-radius circles. Third, we have changed the semantics of the forces used in the model, some of which in their paper were artificial, not physically motivated. On the other hand, it is exactly the modelling based on forces that makes this model attractive for cell simulations. In fact, the relation between forces and pedestrian positions is in their model, perhaps not knowingly, formulated with the Langevin equation [20], which is used to model Brownian motion of particles and is also used for modeling motion of cells [25].

1.3 Contribution of This Paper

In this paper we propose a simple to use yet versatile method[1] to generate GT-enabled image sequences with vast amounts of cells which show various tracking events:

- cells move and change shape (as an inevitable property of live),
- they may have contact and can even overlap slightly (simulates dense populations),
- they split due to cell divisions (simulates mitosis),
- they disappear due to cell death (simulates starvation due to excessive forces acting on them) or as they leave the image (simulates leaving the observed field of view),
- they appear after the mitosis or enter the image again.

The method works with 2D masks of all common biomedical shapes, including those of nuclei and cells themselves. The method is primarily designed to operate at inter-cellular scope, not at the intra-cellular scope.

We leave the simulated time-lapse development of cell internal structure, the cell texture, in the first phase (I) as well as the simulation of second (II) and third (III) phases to the user — a developer of tracking algorithm for her particular application. It is precisely this application that dictates what texture should be used and how images of the cells will be further altered to simulate the image acquisition. We suggest that developers of the tracking algorithms substitute their masks with the output of the proposed method in order to obtain yet more intricate tracking tasks, for which complete tracking GT is available, see Fig. 1.

2 Method

2.1 Cell Motion

Each cell i is represented with its centre $\boldsymbol{x}_i(t)$ and polarity vector $\boldsymbol{p}_i(t)$, both with respect to the fixed image coordinates, and with a list of polar coordinates of

[1] The implementation is freely available at http://cbia.fi.muni.cz/projects/tragen.html

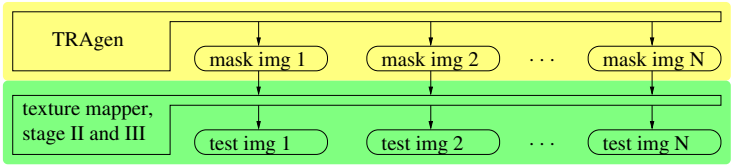

Fig. 1. Scheme of a complete image sequence generator. The output, a sequence of labelled image masks, from the proposed method is submitted to a user supplied SW that overlays the masks with proper texture, yielding a sequence of testing images.

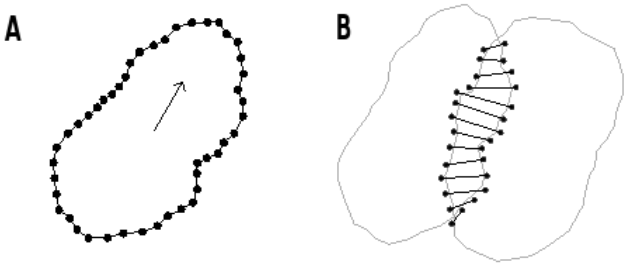

Fig. 2. A) Illustration of a 2D cell representation with emphasized boundary points and the polarity vector placed in the cell centre. Border lines between points are straight. B) Illustration of an (exaggerated) contact of two cells (gray contour) with recognized collision point pairs (solid lines) of the extended boundary. Their number $cp_{i,j}(t, \triangle_f)$ approximates the length of boundary in contact; the length of the longest pair is $-\boldsymbol{d}_{i,j}(t)$.

points representing a cell boundary. The boundary points are treated relatively to the cell centre, see Fig. 2A, and are sorted according to the angular element. The parameter t represents simulated time measured in minutes. We consider any spatial or distance parameters in units of micrometers.

The method utilizes a concept of several types of forces acting on every cell, which conducts motion as a result of it. In fact, it is a purely mechanical model of cell motion. We assume cells are rigid and forces act in their centres. The change of position of a cell is, therefore, characterized with the differential equations:

$$\frac{d\boldsymbol{x}_i(t)}{dt} = \boldsymbol{v}_i(t), \qquad m_i \frac{d\boldsymbol{v}_i(t)}{dt} = \boldsymbol{F}_i(t), \tag{1}$$

where $\boldsymbol{v}_i(t)$ is an instantaneous velocity at time t, m_i is a mass of the cell, and $\boldsymbol{F}_i(t)$ is a sum of individual forces (described below) acting on it at time t. We solve this system with the standard Euler method with time step of 0.1 minutes.

In order to push cell i to move, we introduce two forces:

$$\boldsymbol{F}_i^{desired}(t) = m_i \ \boldsymbol{v}_i^d(t)/\tau_p \ , \tag{2}$$

$$\boldsymbol{F}_i^{friction}(t) = -m_i \ \boldsymbol{v}_i(t)/\tau_p \ . \tag{3}$$

The force $\boldsymbol{F}_i^{desired}(t)$ represents total force exerted by a cell when conducting standard actin-induced adhesion-based motion [1]. This force is driven with a desired velocity $\boldsymbol{v}_i^d(t)$ and a persistence time τ_p, that is, how long on average the cell keeps moving in the same direction and with the same speed until a change occurs. Following this definition, we keep changing the desired velocity (direction and speed) after normally-distributed random period of time; hence $\boldsymbol{v}_i^d(t)$ is a function of time. To counterbalance this motion-inducing force, as in standard mechanics any object keeps accelerating as long as result of forces acting on it is not zero, we consider a friction force $\boldsymbol{F}_i^{friction}(t)$. This force can be understood as a drag when cell is moving in a viscous environment; it also allows cell to decelerate when required. Changing of the desired velocity corresponds to the random terms that yield Brownian-like motion in the Langevin equation [20,25].

To accommodate for mutual inter-cellular interactions, let us first define $\boldsymbol{n}_{i,j}(t) = (\boldsymbol{x}_j(t) - \boldsymbol{x}_i(t))/|\boldsymbol{x}_j(t) - \boldsymbol{x}_i(t)|$, the unit vector pointing from the cell i centre toward the centre of the cell j at time t, and a signed distance $\boldsymbol{d}_{i,j}(t)$ between boundaries of the two cells: it is minimal Euclidean distance between boundary points when the cells do not overlap, otherwise it is maximum distance of the boundary point pairs in the overlap times minus one (-1), see Fig. 2B. Finally, the following forces, adapted from [9], are calculated:

$$\boldsymbol{F}_i^{repulsive}(t,j) = \boldsymbol{n}_{j,i}(t)\ max(\boldsymbol{d}_{i,j}(t),0)\ Ae^{-\boldsymbol{d}_{i,j}(t)/B}\ , \tag{4}$$

$$\boldsymbol{F}_i^{body}(t,j) = \boldsymbol{n}_{j,i}(t)\,(max(-\boldsymbol{d}_{i,j}(t) - \triangle_o, 0)\ k + max(-\boldsymbol{d}_{i,j}(t),0)\ A)\,, \tag{5}$$

$$\boldsymbol{F}_i^{sliding}(t,j) = \boldsymbol{n}_{i,j}^{\perp}(t)\ max(-\boldsymbol{d}_{i,j}(t),0)\ \kappa\ \boldsymbol{n}_{i,j}^{\perp}(t)\cdot(\boldsymbol{v}_j(t) - \boldsymbol{v}_i(t))\ , \tag{6}$$

$$\boldsymbol{F}_i^{attractive}(t,j) = \boldsymbol{n}_{i,j}(t)\ decay_{i,j}(t,\tau_a)\ C(1 + cp_{i,j}(t,\triangle_f))\ . \tag{7}$$

The operator $max()$ serves as a unit-less cut-off operator such that, for instance, the force $\boldsymbol{F}_i^{repulsive}(t,j)$ is effective only when there is no collision between the two cells. Note that orientations of forces differ; the $\boldsymbol{n}_{i,j}^{\perp}(t)$ is a unit vector perpendicular to $\boldsymbol{n}_{i,j}(t)$.

The repulsive force $\boldsymbol{F}_i^{repulsive}(t,j)$ corresponds to an increasing effort of an approaching cell to expel all material between the two cells so that they can touch eventually. This force can be also understood as a force to slow down the approaching cell before the contact. Once the contact occurs, the sliding force $\boldsymbol{F}_i^{sliding}(t,j)$, altered with the parameter κ, is in effect. Its task is to equal velocities of the cells in contact. The counter-deformation force $\boldsymbol{F}_i^{body}(t,j)$ permits a decent overlap of a distance $\triangle_o$ micrometers. If, however, the overlap of cells increases, this force increases proportionally as well. Since the overlap mimics non-rigid deformation of the cell, by adjusting the rate k, one can control cell stiffness and consequently the amount of deformation and thus overlap allowed.

The purpose of the attractive force $\boldsymbol{F}_i^{attractive}(t,j)$ is to keep neighboring cells together. The strength of the connection is proportional to the length of the coinciding boundary extended by $\triangle_f$ micrometers between the cells i and j. This is expressed with $cp_{i,j}(t,\triangle_f)$, see Fig. 2B, as the number of extended boundary point pairs in the cell overlap. The extension $\triangle_f$ of the boundary corresponds to the length of cell filaments which many cells use to sense others within their close

spatial vicinity. In order to allow a cell to escape from a cluster, we introduce the term $decay_{i,j}(t, \tau_a) \in \{0, 1\}$ that goes to 0 whenever there is no contact between the two cells within the period of time τ_a, i.e., $\forall t' \in \langle t - \tau_a, t \rangle : cp_{i,j}(t', \triangle_f) = 0$. During this period, decent force $\boldsymbol{F}_i^{attractive}(t', j) = C$ still applies, and then vanishes completely.

Last but not least, we consider the force $\boldsymbol{F}_i^{boundary}(t) = Ae^{-\boldsymbol{db}_i(t)/B}$ where $\boldsymbol{db}_i(t)$ is the distance to the closest image boundary. The force acts perpendicularly away from it. This (artificial) force is an optional aid to keep cells within the simulated field of view.

If any of $\boldsymbol{F}_i^{repulsive}(t, j)$, $\boldsymbol{F}_i^{body}(t, j)$, or $\boldsymbol{F}_i^{sliding}(t, j)$ keeps exceeding a threshold value $\boldsymbol{F}_{max}$ over a period of 5% of the cell cycle (the length of the mitosis), the cell is assumed not to sustain the force and is, thus, removed from simulation.

2.2 Cell Shape Changes

In order to allow for realistic simulation of long-term observations, longer than is the duration of one cell cycle of the simulated cells, we suggest to implement cell division. The cell cycle is split into several phases [19]. From the shape changes perspective, the significant ones are Telophase, Cytokinesis and G1-phase, during which a mother cell elongates before the division, the division happens, and daughter cells grow after the division, respectively. Given that the boundary points are represented in polar coordinates with respect to the cell centre, we just iteratively extend distance elements in all boundary points by a constant or by Gaussian-shaped function centered along axis of elongation to mimic cell growth or cell elongation, respectively. The elongation axis coincides with the polarity vector $\boldsymbol{p}_i(t)$. For the division, we first iteratively decrease the distances by narrow Gaussian-shaped function centered along axis of division which is perpendicular to the axis of elongation, and split the boundary point list into new lists of two daughter cells in the end.

Furthermore, it is established that many cells (but not all, e.g., keratocytes) tend to maintain polarity and move along this direction. To simulate this, we smoothly rotate the cell around its centre such that the angle between the current polarity $\boldsymbol{p}_i(t)$ and desired velocity $\boldsymbol{v}_i^d(t)$ vectors is minimized.

To summarize the simulation, we first adjust shape of every cell in the system, then we calculate forces, and solve eq. (1) afterwards. Note that this enables a user to inject one's own cell mask instead of having the shape adjusted as described above. In this way, one can fully control the mask shapes, e.g., employ one's own complex non-rigid shape changes [5,26], while have the masks moving and interacting during the simulation.

3 Results

The parameters of the simulations are summarized in Table 1. Initial number of cells was always 64 and were spread in a 8-by-8 grid with initial desired speed of $0\mu\text{m}\,\text{min}^{-1}$. The diameter of cells along the polarity vector was 20µm.

Table 1. Summary of values used in this paper. The notation $\langle a, b\rangle$ denotes uniformly distributed random value between the numbers a and b.

$m_i = 1\text{mg}$	$\tau_p \in \langle 10, 20\rangle\text{min}$	$\boldsymbol{v}_i^d(t) \in \langle 0.0, 0.8\rangle\mu\text{m min}^{-1}$
$A = 0.1\text{N}$	$B = 0.6\mu\text{m}$	$\boldsymbol{F}_{max} = 0.3\text{N}$
$k = 0.2\text{N}$	$\kappa = 0.3\text{N min}\,\mu\text{m}^{-1}$	$\delta_o = 0.5\mu\text{m}$
$C = 0.02\text{N}$	$\tau_a = 10\text{min}$	$\delta_f = 0.5\mu\text{m}$

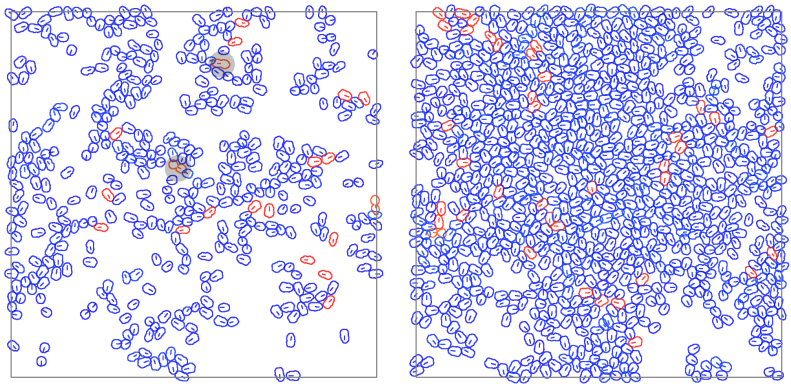

Fig. 3. Comparison of synthetic medium-dense (in the left) to dense (in the right) populations of cells. There are 418 and 955 cells displayed. The cells in red are in mitosis, those in blue are not. Note in the left image the two outlined cells that are in the process of cell division. Images were dilated by 1px for displaying purposes.

The complete cell cycle duration was set to 300min, with 0.4%, 0.4% and 50% of it allocated for the cell elongation, division, and growth, respectively. The system was computing with temporal resolution of 0.1 simulated minutes. The frequency of rendering cells into a sequence of images, the temporal sampling of the sequence, is a user parameter. Spatial resolution is limited only by machine floating-point precision as the coordinates were real-valued, presumably in units of µm. Similarly, spatial image resolution, DPI, is a user parameter as well.

We show here four snapshots of simulations, and encourage interested reader to download and try the method. The snapshots focus on the prominent problem in the tracking task: the linking of touching objects between consecutive images. Note that segmentation of images is not addressed in this paper. In Fig. 3, we compare medium-dense population of cells, where some had already formed tight clusters, to dense, tissue-like cell configuration. In this case, the force $\boldsymbol{F}_i^{boundary}(t)$ was used. The death-inducing threshold $\boldsymbol{F}_{max}$ was, however, set very high so that it effectively prohibited cells to get removed, yielding tight over-populated configuration of cells under increased stress (stress figures not shown). In Fig. 4, boundary force was not used and $\boldsymbol{F}_{max}$ was set as reported in the table. Notice relaxed packing configuration in the right image.

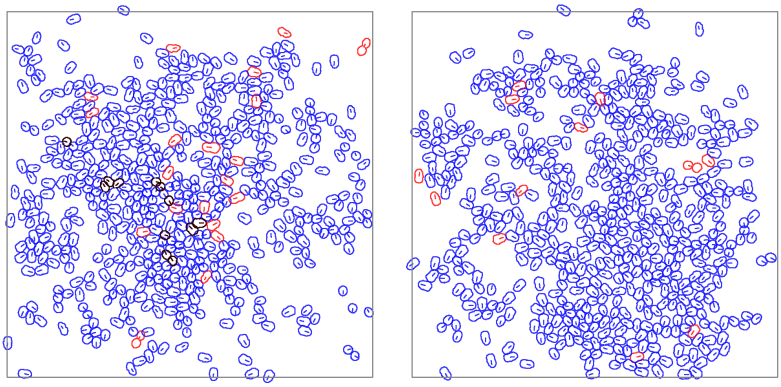

Fig. 4. Comparison of synthetic populations of 551 (in the left) and of 553 (in the right) cells with disabled (in the left) and enabled (in the right) removing of cells due to exceedingly strong forces acting on them. The black cells suffer from the excessive force. Images were dilated by 1px for displaying purposes.

The time complexity of the method when generating next image in the sequence is quadratic with respect to the number of simulated cells, because it needs to calculate mutual distances between all the cells. The most demanding operation is to compute $cp_{i,j}(t, \triangle_f)$. The time complexity is independent of the size of the generated images. Total time required to calculate positions of 300 cells in 100 frames on a standard desktop PC was less than 1 minute (single threaded implementation).

3.1 Case Study: Comparison Against Real Annotated Data

In order to demonstrate that the method can be adapted to simulate a particular and non-trivial real tracking data, we will compare generated sequences against a real sequence of Pancreatic Stem Cells on a polystyrene substrate[2]. It is a sequence of 2D images showing single-isolated motile cells to small clusters, 150–300 cells in an image, acquired in a sequence of 100 images sampled every 10 minute, and observed with the phase-contrast microscopy, see Fig. 5.

To mimic the sequence, we adjusted the initial number, initial positions and the desired speed of all cells as well as the size of the output images to meet spatial parameters, the total simulated time and sampling to meet temporal parameters, and complete cell cycle duration to meet the population growth rate, see Fig. 6. Finally, we have implemented provisional texture mapper, that used the produced masks as described earlier in this paper (e.g., Fig. 1), to obtain a visually similar sequence, see Fig. 5.

[2] Data was obtained with permission from the Cell Tracking Challenge web site http://www.codesolorzano.com/celltrackingchallenge/, courtesy of Dr. Tim Becker.

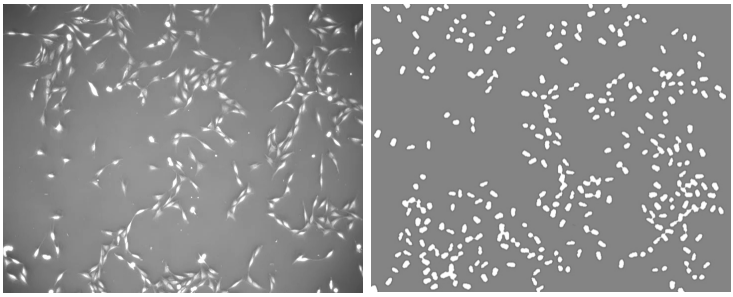

Fig. 5. Sample image from the real (in the left) and synthetic (in the right) sequence.

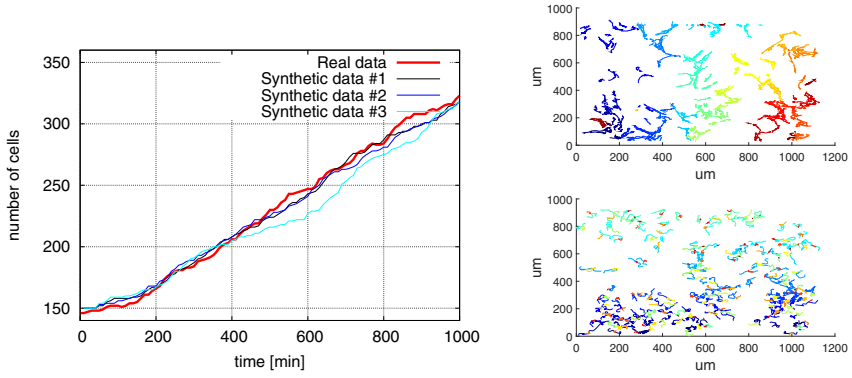

Fig. 6. In the left, comparison of the development of the number of cells over time. The growth rate of the simulated population appears to mimic the one in the real data. In the right, comparison of the cell tracks. The motility of synthetic cells (bottom) appears rather similar to the real ones (top).

4 Conclusion

We have described a method, which is both simple to use and control yet versatile in the variety of simulated aspects. It can simulate, for instance, motile isolated cells, cells preferring to form clusters, or tissue-like cell cultures during complete cell cycle including the cell division. One can control the rate of cell divisions, average speed of cells, and temporal sampling of the simulation to steer complexity of the tracking task. It is designed to provide a sequence of 2D images with labelled masks together with lineage trees that serves as a complete tracking GT data, all in the format adopted in the Cell Tracking Challenge [16]. We believe that prospective authors of next tracking algorithms may easily add appropriate textures [10,15] to these masks and tailor appearance of the obtained testing images specifically to the context of their needs, e.g., to phase-contrast or fluorescence microscopy, or to images with different SNR. The testing images

obtained in this way, can become yet more realistic and thus more relevant for the evaluation.

The method is primarily designed to operate at inter-cellular scope, not at the intra-cellular scope. It is, however, possible to extend it such that it can work even with masks of particles, e.g., genes, or some smaller intra-cellular structures such as protein territories or mitochondria, provided forces are adapted appropriately or new ones are introduced, e.g., a force keeping genes within the same cell.

Given the results of this report, that the adopted force-based approach is viable for 2D time-lapse cell simulations, we plan to extend the simulations into a full 3D time-lapse including non-rigid deformations of the 3D cells. The simultaneous movement and deformation of cells should be a result of mechanical model of a viscoelastic cell after collecting various forces acting on it.

Acknowledgments. This work was supported by Czech Science Foundation — grant No. GA14-22461S.

References

1. Ananthakrishnan, R., Ehrlicher, A.: The forces behind cell movement. International Journal of Biological Sciences **3**(5), 303–317 (2007)
2. Buck, T., Li, J., Rohde, G., Murphy, R.: Toward the virtual cell: Automated approaches to building models of subcellular organization "learned" from microscopy images. Bioessays **34**(9), 791–799 (2012)
3. Coelho, L.P., Shariff, A., Murphy, R.F.: Nuclear segmentation in microscope cell images: A hand-segmented dataset and comparison of algorithms. In: ISBI, pp. 518–521 (2009)
4. Dufour, A., Shinin, V., Tajbakhsh, S., Guillen-Aghion, N., Olivo-Marin, J.C., Zimmer, C.: Segmenting and tracking fluorescent cells in dynamic 3-D microscopy with coupled active surfaces. IEEE Trans. on Image Processing **14**(9), 1396–1410 (2005)
5. Dufour, A., Thibeaux, R., Labruyere, E., Guillén, N., Olivo-Marin, J.: 3-D active meshes: fast discrete deformable models for cell tracking in 3-D time-lapse microscopy. IEEE Trans. on Medical Imaging **20**(7), 1925–1937 (2010)
6. Duives, D.C., Daamen, W., Hoogendoorn, S.P.: State-of-the-art crowd motion simulation models. Transportation Research Part C: Emerging Technologies **37**, 193–209 (2013)
7. Dzyubachyk, O., van Cappellen, W.A., Essers, J., Niessen, W.J., Meijering, E.: Advanced level-set-based cell tracking in time-lapse fluorescence microscopy. IEEE Trans. on Medical Imaging **29**(3), 852–867 (2010)
8. Gelasca, E.D., Byun, J., Obara, B., Manjunath, B.: Evaluation and benchmark for biological image segmentation. In: ICIP, October 2008
9. Helbing, D., Farkas, I., Molnar, P., Vicsek, T.: Simulation of pedestrian crowds in normal and evacuation situations. Pedestrian and Evacuation Dynamics **21**, 21–58 (2002)
10. Lehmussola, A., Ruusuvuori, P., Selinummi, J., Huttunen, H., Yli-Harja, O.: Computational framework for simulating fluorescence microscope images with cell populations. IEEE Trans. Med. Imaging **26**(7), 1010–1016 (2007)

11. Li, K., Miller, E., Chen, M., Kanade, T., Weiss, L., Campbell, P.: Cell population tracking and lineage construction with spatiotemporal context. Medical Image Analysis **12**(5), 546–566 (2008)
12. Lihavainen, E., Mäkelä, J., Spelbrink, J., Ribeiro, A.: Mytoe: automatic analysis of mitochondrial dynamics. Bioinformatics **28**(7), 1050–1051 (2012)
13. Ljosa, V., Sokolnicki, K.L., Carpenter, A.E.: Annotated high-throughput microscopy image sets for validation. Nat. Methods **9**(7), 637 (2012)
14. Magnusson, K., Jalden, J.: A batch algorithm using iterative application of the viterbi algorithm to track cells and construct cell lineages. In: 2012 9th IEEE International Symposium on Biomedical Imaging (ISBI), pp. 382–385, May 2012
15. Malm, P., Brun, A., Bengtsson, E.: Simulation of bright-field microscopy images depicting pap-smear specimen. Cytometry Part A **87**(3), 212–226 (2015)
16. Maška, M., Ulman, V., Svoboda, D., Matula, P., Matula, P., et al.: A benchmark for comparison of cell tracking algorithms. Bioinformatics, pp. 1609–1617 (2014)
17. Perlin, K.: An image synthesizer. In: SIGGRAPH 1985: Proceedings of the 12th Annual Conference on Computer Graphics and Interactive Techniques, pp. 287–296. ACM Press, New York (1985)
18. Rajaram, S., Pavie, B., Hac, N.E.F., Altschuler, S.J., Wu, L.F.: Simucell: a flexible framework for creating synthetic microscopy images. Nat. Methods **9**(7), 634–635 (2012)
19. Reece, J., Urry, L., Cain, M., Wasserman, S., Minorsky, P., Jackson, R.: Campbell Biology, 9th edn. Pearson Benjamin Cummings (2011)
20. Romanczuk, P., Bär, M., Ebeling, W., Lindner, B., Schimansky-Geier, L.: Active Brownian particles. The European Physical Journal - Special Topics **202**(1), 1–162 (2012)
21. Ruusuvuori, P., Lehmussola, A., Selinummi, J., Rajala, T., Huttunen, H., Yli-Harja, O.: Benchmark set of synthetic images for validating cell image analysis algorithms. In: Proceedings of the 16th European Signal Processing Conference, EUSIPCO (2008)
22. Svoboda, D., Ulman, V.: Towards a realistic distribution of cells in synthetically generated 3d cell populations. In: Petrosino, A. (ed.) ICIAP 2013, Part II. LNCS, vol. 8157, pp. 429–438. Springer, Heidelberg (2013)
23. Svoboda, D., Kozubek, M., Stejskal, S.: Generation of digital phantoms of cell nuclei and simulation of image formation in 3d image cytometry. Cytometry Part A **75A**(6), 494–509 (2009)
24. Svoboda, D., Ulman, V.: Generation of synthetic image datasets for time-lapse fluorescence microscopy. In: Campilho, A., Kamel, M. (eds.) ICIAR 2012, Part II. LNCS, vol. 7325, pp. 473–482. Springer, Heidelberg (2012)
25. Szabo, A., Perryn, E., Czirok, A.: Network formation of tissue cells via preferential attraction to elongated structures. Phys. Rev. Lett. **98**, 038102 (2007)
26. Tektonidis, M., Kim, I.H., Chen, Y.C.M., Eils, R., Spector, D.L., Rohr, K.: Non-rigid multi-frame registration of cell nuclei in live cell fluorescence microscopy image data. Medical Image Analysis **19**(1), 1–14 (2015)
27. Webb, D., Hamilton, M.A., Harkin, G.J., Lawrence, S., Camper, A.K., Lewandowski, Z.: Assessing technician effects when extracting quantities from microscope images. Journal of Microbiological Methods **53**(1), 97–106 (2003)
28. Xiong, W., Wang, Y., Ong, S.H., Lim, J.H., Jiang, L.: Learning cell geometry models for cell image simulation: An unbiased approach. In: ICIP, pp. 1897–1900 (2010)